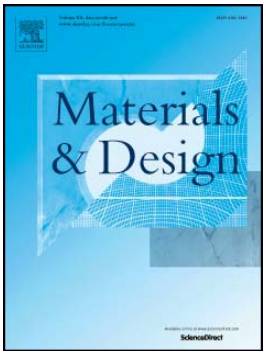

Boron-alloyed Fe-Cr-C-B Tool Steels – Thermodynamic Calculations and Experimental Validation

A. Röttger, J. Lentz, W. Theisen

PII: S0264-1275(15)30406-8
DOI: doi: 10.1016/j.matdes.2015.08.157
Reference: JMADE 565

To appear in:

Received date: 17 April 2015
Revised date: 28 August 2015
Accepted date: 31 August 2015

Please cite this article as: A. Röttger, J. Lentz, W. Theisen, Boron-alloyed Fe-Cr-C-B Tool Steels – Thermodynamic Calculations and Experimental Validation, (2015), doi: 10.1016/j.matdes.2015.08.157

Boron-alloyed Fe-Cr-C-B Tool Steels – Thermodynamic Calculations and Experimental Validation

A. Röttger[1)], J. Lentz[1)2)], W. Theisen[1)]

[1]Lehrstuhl Werkstofftechnik, Ruhr-Universität Bochum, 44801 Bochum, Germany

[2]Corresponding author, e-mail: Lentz@wtech.rub.de

Abstract

This study focuses on the development of boron-alloyed tool steels. The influence of Cr additions from 0 to 10 mass% on microstructural changes were investigated for a constant metalloid content (C+B=2.4 mass%). In the first step, thermodynamic calculations were performed to map the quaternary Fe-Cr-C-B system. In the second step, thermodynamic calculations were validated with laboratory melts that were investigated with respect to the microstructure and phase composition. The results of thermodynamic calculations correspond to real material behavior of Fe-Cr-C-B alloys. Furthermore, the influence of chromium on hard phase formation was investigated by means of phase analysis methods, X-ray diffraction (XRD), and energy dispersive spectrometry (EDS). Nanoindentation was used to determine hard phase properties (hardness, Young's modulus). It was shown that chromium promotes the formation of M_2B-type borides. An increase in the Cr content within the M_2B phase led to a transformation from the tetragonal structure into an orthorhombic structure. This transformation is accompanied by an increase in hardness and in the Young's modulus. In contrast, Cr also promotes the formation of Cr-rich carboborides of type $M_{23}(C,B)_6$. However, an increased Cr content within the $M_{23}(C,B)_6$ phase is not associated with an increase in hardness or elastic modulus.

Keywords: steel development; boron; tool steel; Fe-Cr-C-B; hard phase properties; CALPHAD;

1. Introduction

Wear by abrasion limits the durability of tools and machines in the fields of mining, transportation, processing, and machining of materials such as minerals, plastics, and metals. To increase the economic efficiency of a value chain, the durability of tools can be improved by using materials with optimized tribomechanical properties. The essential properties for these applications are a high wear resistance in combination with a sufficient level of toughness. A good compromise for these two opposing requirements is achieved by a

microstructure consisting of a tough metallic matrix and a sufficient amount of a finely dispersed hard phase. In this case, the wear resistance is primarily determined by the properties of the hard phases because they counteract grooving of the metal matrix by abrasives. To achieve a high wear resistance, the hard phases should be individually adapted to the tribological system and especially to the interaction with the abrasive objects. Thus the most important parameters influencing the performance for wear protection applications are parameters that are related to the hard phases, such as hardness, size, volume fraction, type, and morphology. In contrast to direct wear protection by hard phases, the metallic matrix provides toughness and a basic strength to support the embedded hard phases.

A comparison of the hardness of carbides, nitrides, and borides with the same stoichiometry shows that borides generally possess the highest hardness. For example, Fe_3C in Fe-C alloys has a hardness of about 1100 HV [1]. In contrast, the hardness of boron cementite (Fe_3B) in ternary Fe-C-B alloys is in the range of 1000 to 1600 HV0.05 [2–4]. This greater hardness of boron cementite can be attributed to stronger M-B bonding, which was shown by the ab initio calculations of Shein et al. performed on Fe_3C and Fe_3B [5]. The comparison between the hardness of borides and carbides suggests utilization of borides as hard phases to achieve materials with a high wear resistance. This approach is well understood and technically utilized to form hard FeB- and Fe_2B-type boride layers in case of thermochemical surface techniques such as boriding or to form Mo- and Cr-rich borides in case of high boron additions in hardfacing alloys [6–9].

Fe-C-B alloys may contain Fe-rich borides (Fe_2B), carboborides ($Fe_3(C,B)$, $Fe_{23}(C,B)_6$), and cementite (Fe_3C) [10,11]. The presence of the respective phases depends on the boron/boron-carbon ratio (B/(B+C)). In the case of a high B/(B+C) ratio, the Fe_2B phase is stabilized, whereas in the direction of a lower B/(B+C) ratio, boron cementite and the τ-phase ($M_{23}(C,B)_6$) become more stable. The Fe_2B phase, in particular, is of great interest in the development of boron-alloyed Fe-base hardfacing alloys and tool steels. The Fe_2B phase offers a high hardness (~1200-1500 HV0.05) and a low carbon solubility (~2 at.%). Thus carbon is uncoupled from hard phase formation and can be used for martensitic hardening of the metal matrix. However, to achieve hard phase formation with boron and martensitic hardening with carbon, the formation of carboborides ($M_3(C,B)$, $M_{23}(C,B)_6$) or carbides has to be suppressed. The formation of carboborides can be prevented by stabilizing the M_2B phase with elements such as chromium or manganese and simultaneous use of a high B/(B+C) ratio of ~0.75. Goldfarb et al. investigated the stabilizing effect of Cr addition on the formation of a Cr-rich M_2B phase [12]. They explained that the M_2B phase is formed during disintegration of the metastable $(Fe,Cr)_3B$ phase, which is mostly formed during rapid non-

equilibrium solidification. Eutectic formation of the $Fe_3(B,C)$ phase was followed by a M_2B transformation. Furthermore, the amount of Cr also affects the stability of the Fe-rich tetragonal M_2B phase (subsequently named $(Fe,Cr)_2B$)). If chromium exceeds the solubility limit of $(Fe,Cr)_2B$ (~16-20 at%), Fe-rich tetragonal $(Fe,Cr)_2B$ transforms by atomic substitution into orthorhombic Cr-rich M_2B (subsequently named $(Cr,Fe)_2B$), which has a higher solubility for Cr (~72 mass%) [13,14]. This type of transformation was also confirmed by the work of Dybkov et al. and Ma et al. [15,16]. Ma et al. also investigated changes in the mechanical properties of the M_2B phase as a function of the chromium content. They found an increase in hardness and fracture toughness on increasing the Cr content in the M_2B phase in cast Fe-3.5B alloys by varying the Cr content of the alloy (0-15 mass%). The hardness of the $(Fe,Cr)_2B$ phase was initially increased constantly from 1350 HV0.1 (0 mass% Cr) to 1500 HV0.1 (8 mass% Cr). Above an overall Cr content of 12 mass%, the orthorhombic phase $(Cr,Fe)_2B$ was present, and the hardness as well as the fracture toughness of this boride were greatly increased to ≥1690 HV0.1 and ≥ 20 MPa√m, respectively.

In comparison, orthorhombic Cr-rich borides of type $(Cr,Fe)_2B$ possess equal or better tribomechanical properties than the Cr-rich carbides M_7C_3 (hardness ~1400 to 1600 HV0.05, K_1c ~6.3 MPa√m) and $M_{23}C_6$ (hardness ~1150 to 1450, K_1c ~4.4 MPa√m), which are formed in tool steels and white cast irons based on the ternary Fe-Cr-C system [17,18]. Therefore, utilization of boron as a hard phase-forming element represents a promising way to enhance the tribomechanical properties of wear-resistant Fe-base alloys. The motivation of this study is to investigate the influence of Cr addition on the formation of borides and carboborides in Fe-Cr-C-B alloys with regard to the hard phase properties (hardness and Young's modulus) and thus provide a first guide for the development of Fe-base alloys containing borides as hard phases. In this work, the initial alloy was defined as a Fe-C-B alloy with a constant metalloid content (C = 0.7 mass%; B = 1.8 mass%) and the Fe_2B-stabilizing elements silicon and manganese. The influence of Cr addition on the phase composition was investigated by means of thermodynamic calculations in the range of 0 to 10 mass% chromium. These thermodynamic calculations were then evaluated by laboratory melts that were heat-treated close to the equilibrium condition and investigated using scanning electron microscopy (SEM) and EDS. Furthermore, the influence of Cr addition on the type and hardness of the resulting hard phases was investigated by nanoindentation.

2. Experimental procedure

2.1 Thermodynamic calculations

Phase diagrams were calculated by thermodynamic equilibrium calculations using the CALPHAD method. Software package Thermo-Calc version S (Thermo-Calc AB, Stockholm,

Sweden) and the TCFe7 database were used to calculate the phase diagrams and the chemical composition of the respective phases in the equilibrium state. The calculations were performed with a phase set reduced to LIQUID, BCC_A2, FCC_A1, CEMENTITE, M7C3, M2B_tetr, Cr2B_orth, and M23C6 and by taking into account a substance quantity of n=1 mol and a pressure of p= 1000 mbar.

2.2 Materials

The laboratory melts (200 g) used for the analysis of the mechanical and crystallographic properties and also for validation of the thermodynamic calculations were cast in a vacuum induction furnace. In the reference state, the selected Fe-based alloys possessed a constant metalloid content of 2.75 mass% with a B/(B+C) ratio of 0.727 to ensure formation of an Fe-rich boride of type M_2B. In addition, the elements manganese and silicon were present with a constant content of 3.8 mass% Mn and 2.35 mass% Si to stabilize formation of the M_2B phase by counteracting the stability of the $Fe_3(C,B)$ phase. Furthermore, chromium was added from 0 to 10 mass% with a constant increment of 2 mass%. The chemical composition of the bulk specimens after casting was measured by optical emission spark spectroscopy (QSG750 spectrometer OBLF) (***Table 1)***.

Table 1: Chemical composition of the laboratory melts measured by optical emission spark spectrometry in mass%

Alloy	C	B	Cr	Si	Mn	N	Fe
FeCB0Cr	0.75	1.98	0.04	2.27	3.81	0.02	bal.
FeCB2Cr	0.74	2.00	1.94	2.25	3.84	0.03	bal.
FeCB4Cr	0.74	2.01	4.10	2.49	3.82	0.01	bal.
FeCB6Cr	0.71	2.02	6.10	2.46	3.79	0.01	bal.
FeCB8Cr	0.72	2.01	8.10	2.46	3.84	0.01	bal.
FeCB10Cr	0.65	1.97	10.00	2.41	3.77	0.01	bal.

2.3 Heat treatment

To compare the thermodynamic calculations and the real microstructure of the laboratory melts, cast specimens were heat-treated to approach the equilibrium state. The heat treatment was performed at 900°C for 200 h in an inert gas furnace in an argon atmosphere, followed by quenching in water.

2.4 Metallography and microscopy

Microstructural examinations were carried out using SEM in the secondary electron and backscattered electron modes with a working distance of 8 to 10 mm and an acceleration voltage of 20 keV. The Cr content of the respective phases in the microstructure was measured using EDS with an acceleration voltage of 10 keV and a working distance of 8 mm. Prior to the microstructural examinations, the specimens were sectioned, ground on abrasive paper, and polished stepwise with 6 µm, 3 µm, and 1 µm diamond suspensions. The final finish was achieved by polishing the specimens with an oxide polishing suspension (0.25 µm) and etching with 3% Nital. Phase analysis was performed by XRD with a Siemens-D500 X-ray diffractometer using chromium K_α radiation and a step size of 0.02°2θ in the range of 50 to 110°2θ. Diffractograms were evaluated with the program ADM (Wassermann) and the JCPDS PDF-2 database.

2.5 Nanoindentation measurements

Measurements of hardness and elastic modulus of the respective hard phase of the laboratory melts were performed by nanoindentation experiments on the polished microstructure using the NHT indentation module (CSM Instruments). Indentation experiments were performed using a Berkovich indenter and a load of 50 mN, which was applied to the specimen within 30 seconds. During testing, force/indentation curves were recorded by the Indentation 4.16 software (CSM Instruments). Indentation hardness and Young's modulus were estimated using the standard method of Oliver and Pharr. For the estimation of Young's modulus, the Poisson ratio of the hard phases was assumed to be a constant value of 0.17. To provide comparability, the indentation hardness was converted to the Vickers hardness number knowing that the minimal depth of indentation according to DIN EN ISO 14577 is not reached. Nevertheless, the identation size effect was found to be negligible with regard to the identation depths obtained in the measurements.

3. Results

3.1 Thermodynamic calculations

Thermodynamic calculations using the CALPHAD method were performed for the boron-alloyed tool steels as a function of Cr content and an initial chemical composition of alloy FeCB0Cr (Fe0.75C2B2.5Si3.8Mn as shown in ***Table 1***).

The quasi-binary phase diagram of the FeCB0Cr alloy as a function of chromium content is shown in ***Figure 1***. Primarily solidification of the γ-Fe phase is followed by the formation of Fe-rich as well as Cr-rich M_2B-type borides, whereby the Cr_2B phase is stabilized by increasing Cr contents. The subsequent solidification path is influenced by the amount of chromium. In the case of a Cr content of up to 3.0 mass%, the low-melting phase is boron cementite ($Fe_3(C,B)$). Above a Cr content of 3.0 mass%, the low-melting phase was calculated to be a Fe-Cr-rich $M_{23}(C,B)_6$ carboboride.

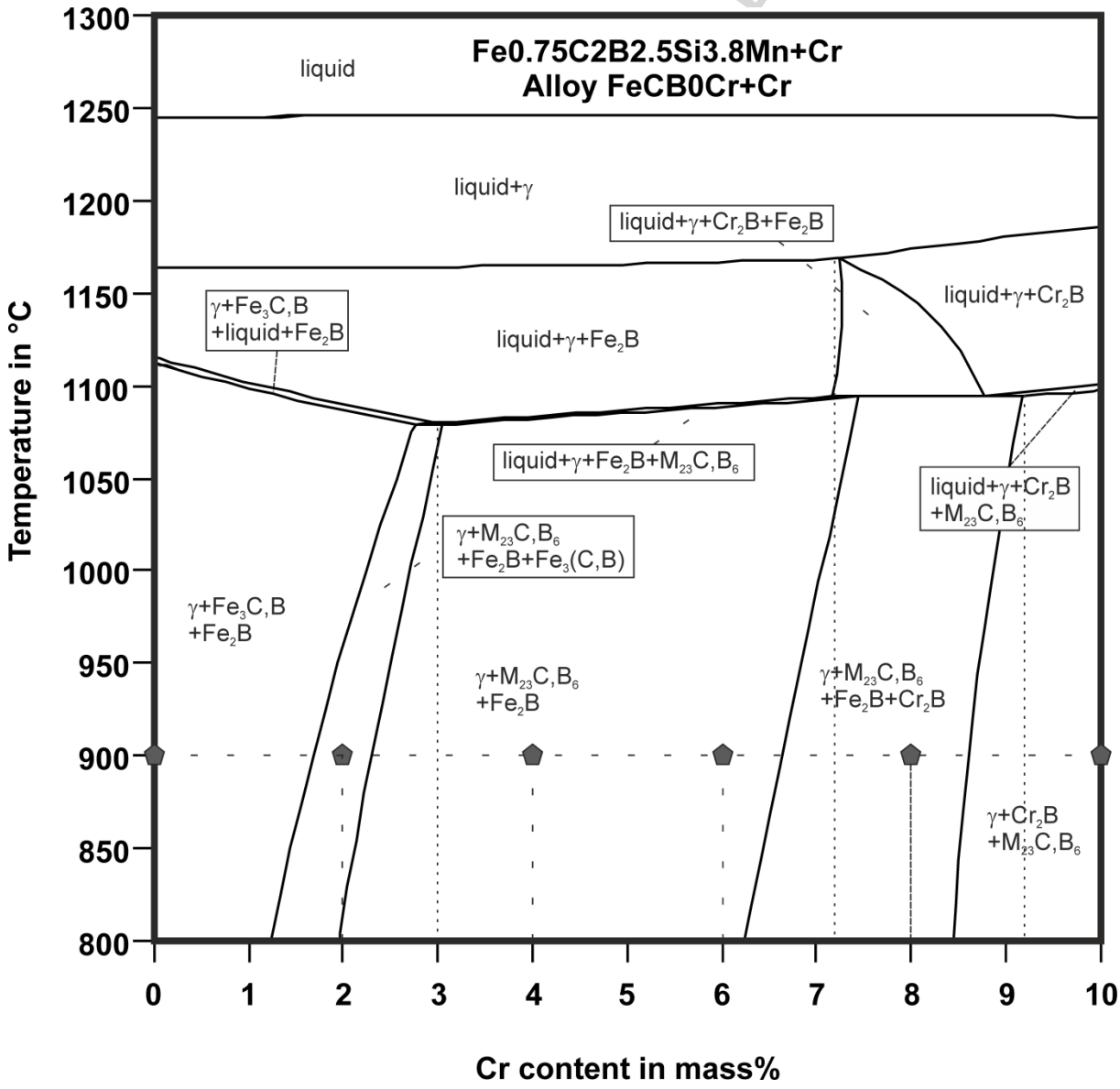

Figure 1: Calculated quasi-binary phase diagram of the FeCB0Cr alloy (Fe0.75C2B2.5Si3.8Mn)

The volume content of the individual phases was calculated as a function of the overall Cr content at 900°C and is depicted in ***Figure 2***. This temperature was chosen with regard to the austenitization temperature and to thus ensure a sufficient C content of 0.5 to 0.7 mass%

in the austenitic phase. ***Figure 2*** shows strong stabilizing effects of Cr on the M_2B and $M_{23}(C,B)_6$ phases. The increase in Cr content increases the volume fraction of the tetragonal $(Fe,Cr)_2B$ phase from 16 vol.% (0 mass% Cr) to 23 vol.% (2.2 mass% Cr). The volume fraction of the $(Fe,Cr)_2B$ phase remains almost constant between a Cr content of 2.2 mass% and 6.8 mass%. A further increase in the Cr content above 6.8 mass% stabilizes the Cr-rich $(Cr,Fe)_2B$ phase with an orthorhombic structure. The volume fraction of the $(Cr,Fe)_2B$ phase increases with a simultaneous decrease in the volume fraction of the Fe-rich $(Fe,Cr)_2B$ phase, whereas the sum of the two M_2B-type phases [$(Fe,Cr)_2B$ + $(Cr,Fe)_2B$] stays at a constant level of 23 vol.%. In the case of the $M_{23}(C,B)_6$ phase, the increase in the volume fraction of $M_{23}(C,B)_6$ is inverse to the decrease in the volume fraction of the $M_3(C,B)$ phase and reaches a constant level of 13 vol.% above 2.2 mass% Cr. At Cr contents above 8.5 mass%, only the γ-Fe, $(Cr,Fe)_2B$, and $M_{23}(C,B)_6$ phases are calculated to be present.

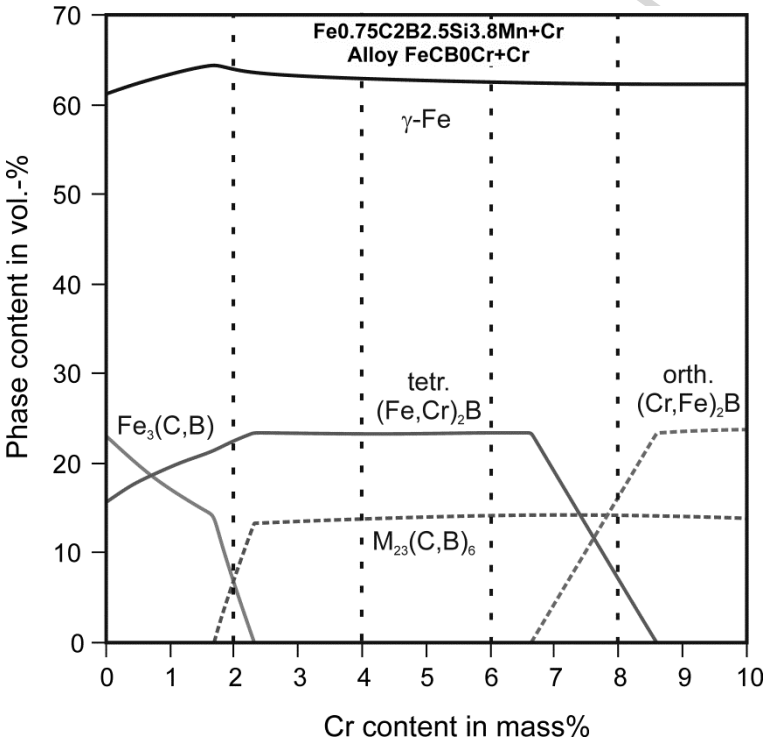

Figure 2: Calculated phase contents as a function of the overall Cr content for the FeCB0Cr alloy (Fe0.75C2B2.5Si3.8Mn) at a temperature of 900 °C

Furthermore, the solute Cr content in the respective phases was calculated as a function of the overall Cr content. The calculation (lines) is depicted in ***Figure 3*** in comparison with EDS measurements (symbols). At a low overall Cr content (<1.8 mass%), Cr is mainly found inside the $(Fe,Cr)_2B$ phase. In the direction of higher overall Cr contents, the amount of solute Cr in the $(Fe,Cr)_2B$, $M_{23}(C,B)_6$, and γ-Fe phases is constantly increasing, and the solute Cr content in the respective phases increases from γ-Fe to $M_{23}(C,B)_6$ to $(Fe,Cr)_2B$. Above an overall Cr content of 6.8 mass%, the solute Cr content in the phases γ-Fe (3

mass%), $(Fe,Cr)_2B$ (15.5 mass%) and $Fe_{23}(C,B)_6$ (12.4 mass%) remains at a constant level and the $(Cr,Fe)_2B$ phase is formed, which has a constant solute Cr content of 26.5 mass%. At an overall Cr content above 8.5 mass%, the solute Cr content in the $(Cr,Fe)_2B$, $M_{23}(C,B)_6$, and γ-Fe phases increases again.

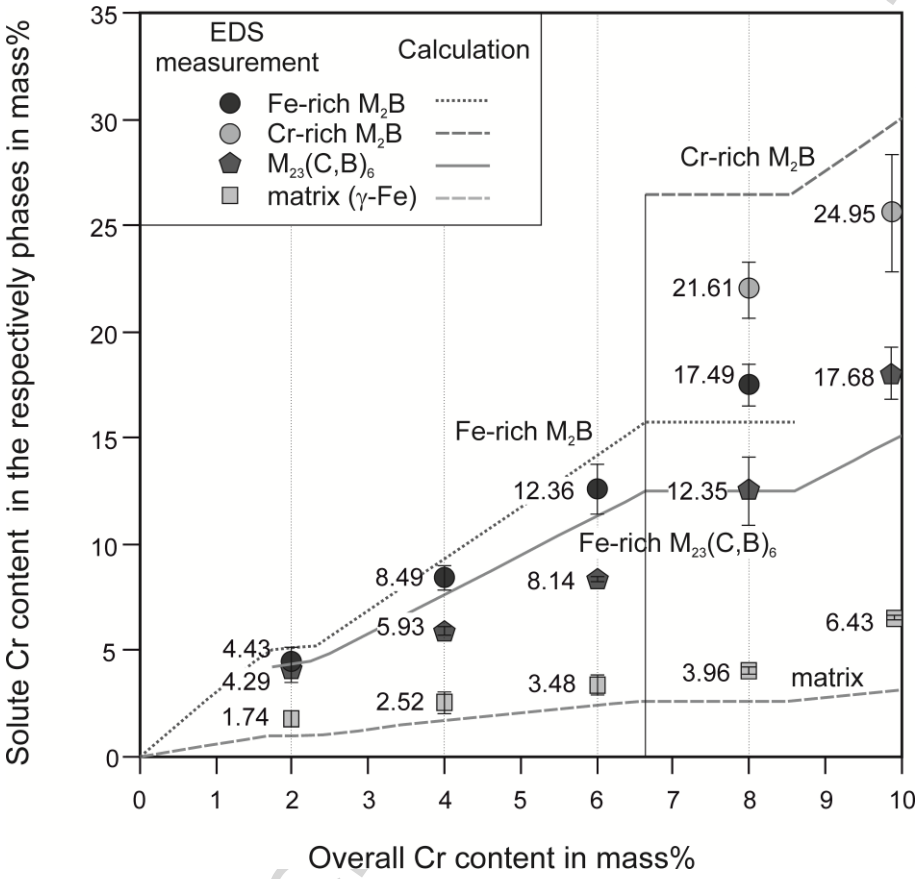

Figure 3: Comparison between calculated and experimental (EDS) Cr contents in the respective phases as a function of the overall Cr content

3.2 Microstructural investigations

The thermodynamic calculations were evaluated by means of laboratory melts. Based on the chemical composition, listed in ***Table 1***, the overall Cr content was increased from 0 to 10 mass% Cr in increments of 2 mass%. The microstructure of the cast material in the annealed condition (200 h, 900°C) was investigated by SEM, as shown in ***Figure 4***. The microstructure of the FeCBCr alloys possesses a metallic matrix in which eutectic hard phases are finely distributed. The volume fraction of the hard phases was estimated quantitatively by optical microscopy using image binarization (a4i-analysis software) to be in a constant range of 35 to 38 vol.% and is independent of the Cr content. This result is also in agreement with the thermodynamic calculations in which the volume fraction of the hard phase was calculated to be nearly constant at around 36 vol.% (***Figure 2***). Differences in the microstructures can be seen in case of the morphology of the eutectic hard phases. The Cr-free alloy consists of two

different hard phases having blocky and coral-like structures, respectively. From the results of EDS investigations, the coral-like structure of the Cr-free FeCB alloy is attributed to the $M_3(C,B)$ phase and the more blocky hard phase morphology is attributed to the M_2B phase. With increasing Cr content (2 mass%), the $M_3(C,B)$ phase diminishes and the FeCr-rich carboboride of type $M_{23}(C,B)_6$ becomes more noticeable. In the case of the alloys having a higher Cr content (4 to 10 mass% Cr), the morphology of the $M_{23}(C,B)_6$-type hard phases can be preferentially described as coral-like. Furthermore, the hard phase of M_2B type possesses a fishbone-like morphology that is independent of the overall Cr content.

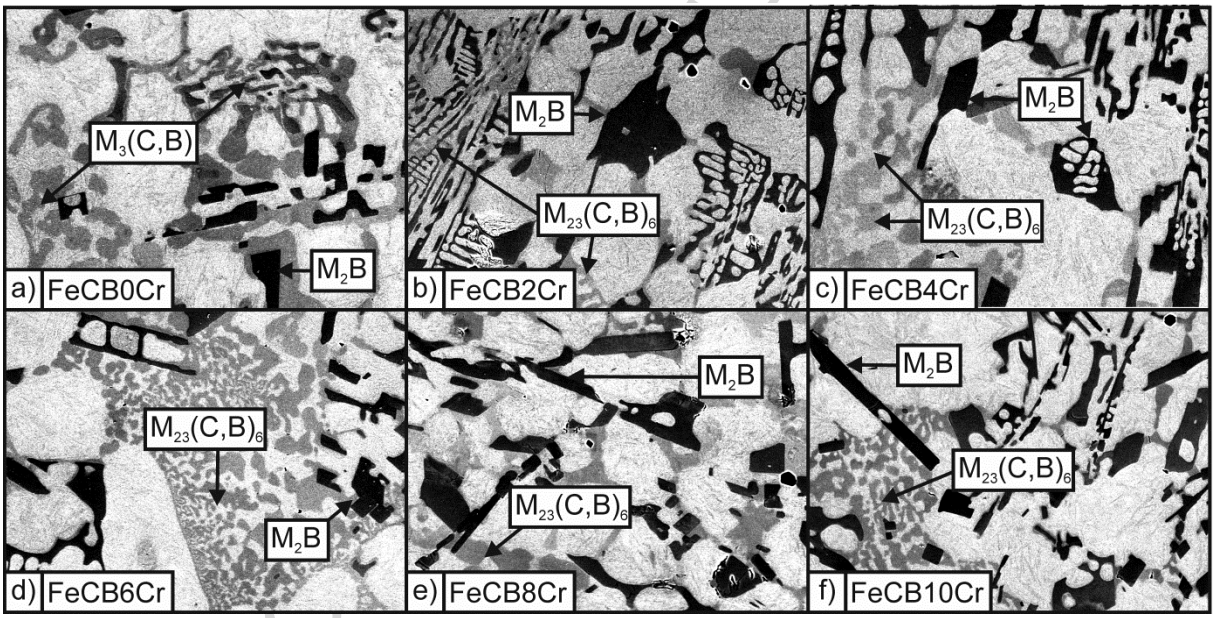

Figure 4: SEM image with BSE contrast of the alloy microstructure (tempered at 900 °C for 200 h and quenched in water)

Phase analysis of the microstructure of the laboratory melts was performed by XRD (see ***Figure 5***). In all cases, the microstructure of the heat-treated specimens consists of a metal matrix containing martensite (α'-Fe) and retained austenite (γ-Fe). Since this work focuses on the influence of Cr addition on the formation of hard phases, the metallic phases (α'-Fe and γ-Fe) will not be taken into account in the following presentation of results and further discussion. In the case of a Cr content below 6 mass%, the results of the phase analysis of the heat-treated specimens correspond to the phases calculated at 900°C by means of CALPHAD method (see ***Figure 2***), Thereby, boron cementite $Fe_3(C,B)$ and Fe-rich $(Fe,Cr)_2B$ were observed in the case of the Cr-free alloy. On increasing the Cr content from 2 to 4 mass%, boron cementite $Fe_3(C,B)$ diminishes and the Fe-rich $M_{23}(C,B)_6$ phase as well as Fe-rich $(Fe,Cr)_2B$ are formed. XRD investigations of the alloy with a higher Cr content of 6 mass% confirm the presence of the Cr-rich $(Cr,Fe)_2B$ phase and also $(Fe,Cr)_2B$. This is in

disagreement with the CALPHAD calculations, which indicate that the Cr-rich $(Cr,Fe)_2B$ phase does not start to form until 6.8 mass% Cr and only Fe-rich $(Fe,Cr)_2B$ should be stable together with the $M_{23}(C,B)_6$ phase. A further increase in Cr content is accompanied by an increase in the amount of Cr-rich $(Cr,Fe)_2B$ phase (encircled in ***Figure 5***) and a decrease in the Fe-rich phase of $(Fe,Cr)_2B$ type. Thus in the alloys having a higher Cr content than 8 mass%, the Cr-rich $(Cr,Fe)_2B$ and $M_{23}(C,B)_6$ phases are again in accordance with the calculated phase composition.

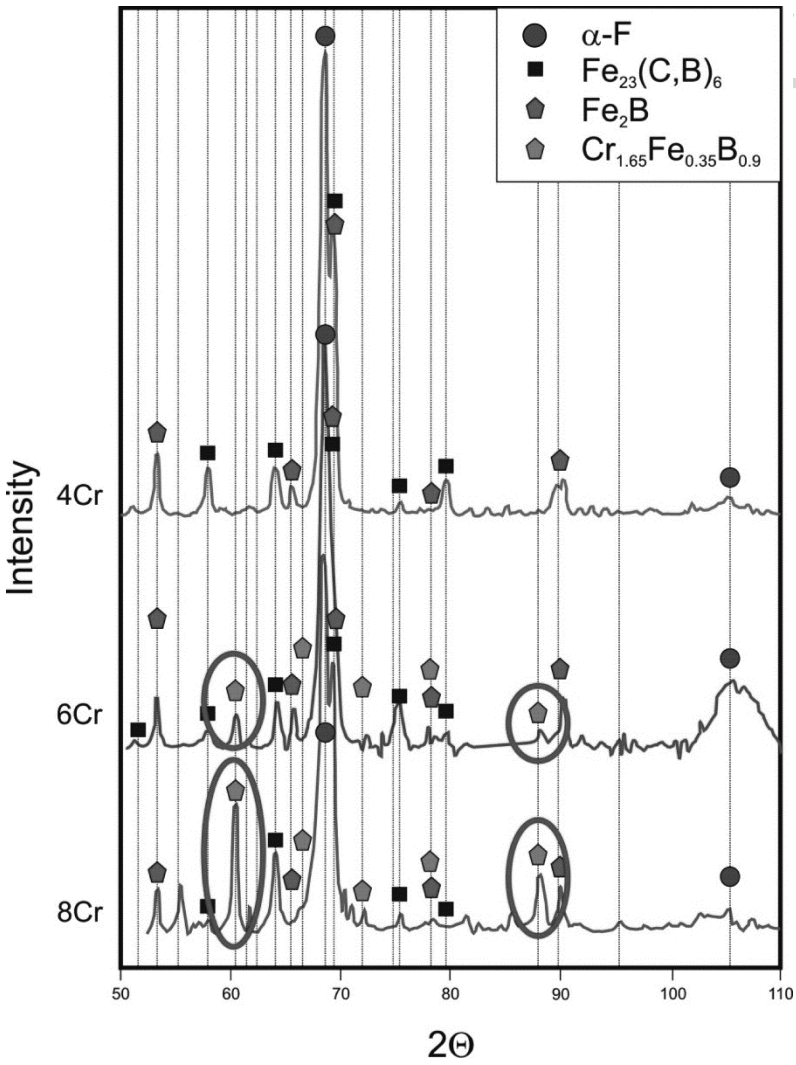

Figure 5: XRD phase analysis of the FeCB4Cr, FeCB6Cr, and FeCB8Cr alloys

3.3 Mechanical properties

Both the hardness as well as the Young´s modulus of the M_2B and $M_{23}(C,B)_6$-type hard phases were evaluated by means of nanoindentation experiments. The hardness of the M_2B and $M_{23}(C,B)_6$ phases as a function of the Cr content is shown in ***Figure 6***. The measured hardness of the $M_{23}(C,B)_6$ phase was in the range of 1100 to 1250 HV, whereby the hardness slightly increases with increasing Cr content. In contrast, a strong influence of the

Cr content on the hardness of the M_2B phase was observed. The measured hardness of the M_2B phase in the Cr-free FeCB0Cr alloy was 1650 HV. In the direction of a higher overall Cr content, the hardness of the M_2B phase increased from 1600 (FeCB2Cr) to 2000 HV (FeCB10Cr).

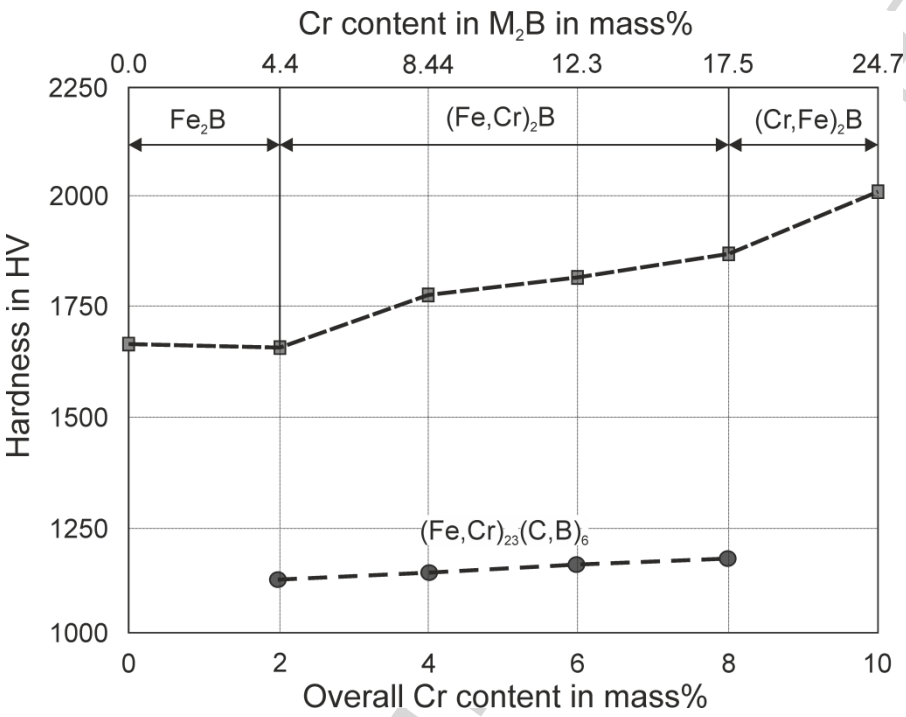

Figure 6: Hardness measured by nanoindentation experiments of the M_2B and $M_{23}(C,B)_6$ phases as a function of the overall Cr content.

The influence of the overall Cr content on Young´s modulus of the M_2B and $M_{23}(C,B)_6$ phases is shown in ***Figure 7.*** The $M_{23}(C,B)_6$ phase possesses an almost constant Young´s modus of between 280 and 300 GPa that is independent of the overall Cr content. In contrast, the Young´s modulus of the M_2B phase rises from 330 to 390 GPa above an overall Cr content of 4 mass%.

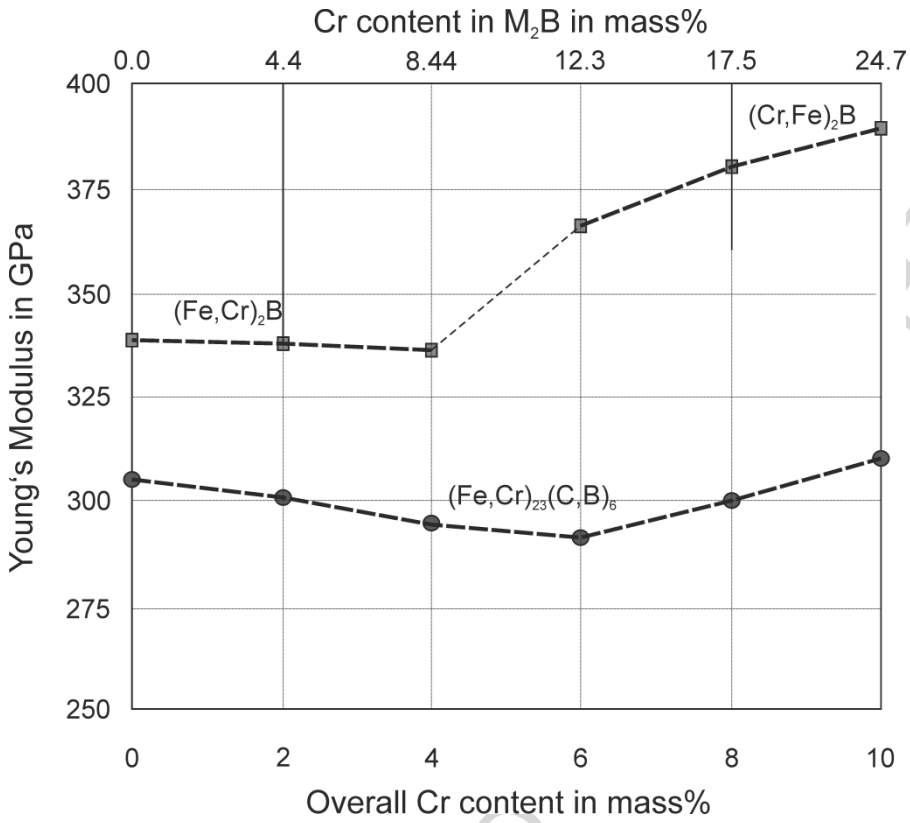

Figure 7: Young's modulus measured by nanoindentation experiments of the M_2B and $M_{23}(C,B)_6$ phases as a function of overall Cr content.

4. Discussion

The microstructure of the analyzed Cr-rich hardfacing alloys possesses a mainly martensitic metal matrix with embedded $M_{23}(C,B)_6$, $M_3(C,B)$, and M_2B type hard phases. Concerning the hypoeutectic alloy composition, primary solidification of metallic dendrites occurs, followed by the formation of the particular hard phases. High B/(B+C) ratios > 0.7 were chosen for the investigated alloys in order to receive a sufficient amount of the M_2B type phases [19]. Thus, this type of hard phase is formed during solidification in a temperature range from 1170 to 1185°C (see ***Figure 1***).

4.1 Microstructure of FeCB alloys having ≤ 3 mass% Cr content

The further solidification path is strongly determined by the amount of added chromium. In the case of a low Cr amount of ≤ 3 mass%, the low-melting eutectic phase was found to be of the $M_3(C,B)$ type. On this account, the solidification sequence of low-Cr FeCB alloys can be explained by a primary solidification of γ-Fe dendrites followed by crystallization of the $(Fe,Cr)_2B$ phase. The remaining melt is enriched in carbon (~1.9 mass% at 1120°C) because of the low solubility of carbon in M_2B phases (close to zero). Although B is forming the

$(Fe,Cr)_2B$ phase with iron, the remaining melt also has an increased boron content (2.7 mass% at 1120°C) because of the continuous crystallization of γ-Fe dendrites, which feature a low solubility for boron (max. 500 ppm). On reaching the respective eutectic concentration, the $Fe_3(C,B)$ phase is formed eutectically within a continuous transition reaction [19]. The calculated phase diagram in ***Figure 1*** shows that the solidus temperature of the $M_3(C,B)$ phase decreases from 1115°C to 1080°C as the Cr content increases from 0 to 3 mass%. This behavior can be attributed to a change in the B/C ratio inside the $Fe_3(C,B)$ phase. In the case of the Cr-free FeCB alloy, the B/C ratio in $Fe_3(C,B)$ was calculated to be 2.83. In contrast, the B/C ratio in the $Fe_3(C,B)$ phase was calculated to be 1.65 for adding 2 mass% Cr in alloy FeCB2Cr. The $Fe_3(C,B)$ phase is thus enriched in carbon and depleted in boron. The decrease in boron content of the $Fe_3(C,B)$ phase with Cr addition can be attributed to the more pronounced stabilization of the M_2B phases. Thus the residual melt is less enriched with boron.

The change of the solidus temperature as a function of the B/C ratio in the $Fe_3(C,B)$ phase was investigated by means of thermodynamic calculations. The calculated solidus temperature of FeCB alloys as a function of the B/C ratio of $Fe_3(C,B)$ phase is shown in ***Figure 8***. As known from the binary Fe-C diagram, the Fe_3C phase crystallizes eutectically at a temperature of 1143°C. With an increase in boron content, the solidus temperature decreases until the eutectic composition of Fe2.3B2.3C is reached at a temperature of 1120°C having a B/(B+C) ratio of 0.5 (see ***Figure 8***). Furthermore, in the direction of a higher boron content in the alloy and inside the $Fe_3(B,C)$ phase (overall B content $\geq$ 2.3 mass%), the solidus temperature increases again. Due to its metastable behavior, pure Fe_3B will not be observed in Fe-B alloys [20]. Schürmann et al. estimated a theoretical melting temperature of 1214°C for Fe_3B [21]. However, Poletti et al. calculated a eutectic temperature of 1147°C for Fe_3B using the CALPHAD method [22]. Therefore, the solidus temperature of hypoeutectic low-Cr FeCB alloys is determined by the B/(B+C) ratio and thus by the chemical composition of the $Fe_3(C,B)$ phase. If the B/(B+C) ratio is higher than 0.85, the tetragonal Fe_2B phase will solidify before $Fe_3(C,B)$ in the melt, which is associated with an increase in solidus temperature.

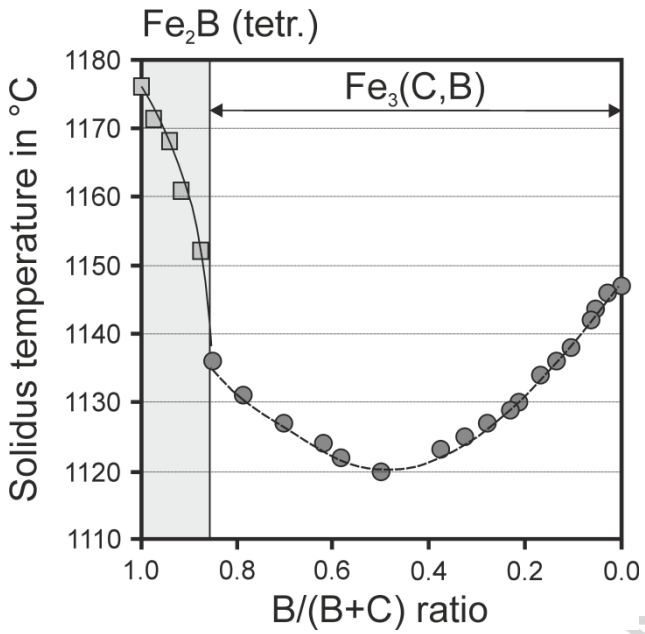

Figure 8: Calculated solidus temperature of the eutectic channel in the ternary Fe-C-B system; calculations were performed using the Scheil-Guliver equation by varying the B/(B+C) ratio between Fe_2B (only B; B/(B+C)= 1.0) and Fe_3C (only C, B/(B+C)= 0.0)

Microstructural investigations confirm the aforementioned solidification sequence of low-Cr FeCB alloys, which is indicated by a blocky Fe-rich M_2B phase (primary solidification) and a $M_3(C,B)$ phase with a coral-like structure (eutectic solidification) as shown in ***Figure 4*** (microstructure of the FeCB0Cr and FeCB2Cr specimens). In the case of the alloy with 2 mass% Cr addition, the $M_{23}(C,B)_6$ phase with a fishbone-like structure is formed together with the M_2B and $M_3(C,B)$-type phases. The thermodynamic calculations (***Figure 1***) show that the transformation of $M_3(C,B)$ + γ-Fe to $M_{23}(C,B)_6$ takes place in the solid state. The γ-Fe + $M_3(C,B) \rightarrow M_{23}(C,B)_6$ transformation is accompanied by an increase in the volume fraction of the hard phases of about 4 vol% from 33 vol% (1000°C) to 37 vol% (800°C). This increase in the overall hard phase volume fraction can be explained by the different metal/metalloid ratio (M/X; X=C+B) in the $M_3(C,B)$ phase [M/X=3] and the $M_{23}(C,B)_6$ phase [M/X= 3.833].

4.2 Formation of the τ phase in FeCB alloys having 3-6 mass% Cr

For the FeCB alloys possessing an overall Cr content higher than 3 mass%, the low-melting eutectic is formed by the $M_{23}(C,B)_6$ phase. The coral-like morphology of the $M_{23}(C,B)_6$ phase can be explained by eutectic crystallization of the $M_{23}(C;B)_6$ phase from the melt instead of a solid-state transformation (see the microstructure of FeCB4Cr, FeCB6Cr, FeCB8Cr, and

FeCB10Cr specimens in ***Figure 4***). The formation and stability of the $M_{23}(C,B)_6$ phase in FeCB alloys is controversially discussed in the literature. On the one hand, authors found the $M_{23}(C,B)_6$ phase to be a metastable phase that is only stable in a limited temperature regime between 900-1000°C in the equilibrium state [21,23]. On the other hand, $M_{23}(C,B)_6$ crystallizing from the melt is often described by constitutional undercooling phenomena. The metastable behavior of $M_{23}(C,B)_6$ was investigated in the work of Borlera et al. and Stadelmaier et al. [24,25]. Borlera et al. found that the τ phase $M_{23}(C,B)_6$ is formed during cooling below a temperature of T = 965°C from the reaction $M_3(C,B)+\gamma\text{-Fe}\rightarrow M_{23}(C,B)_6$. In contrast, Stadelmaier et al. attributed the decomposition of $M_{23}(C,B)_6$ to its instability at temperatures below T = 800°C. They described the decomposition of the τ phase according to the reaction $M_{23}(C,B)_6+M_2B\rightarrow M_3(C,B)+\gamma\text{-Fe}$.

In the following, the stability of the τ phase will be described with respect to the chemical composition and especially to the B/(B+C) ratio of FeCB alloys. Therefore, the influence of the B/(B+C) ratio and Cr addition on the formation of the τ phase will be described with the help of phase diagrams calculated for FeCB ***(Figure 9a*** and ***9b)*** and for FeCrCB alloys ***(Figure 9c*** and ***9d)***. ***Figure 9a*** shows the FeCB phase diagram with 1 mass% carbon. The phase field of the τ phase is grey colored. The calculation shows that the τ phase forms due to a miscibility gap and as a result of the reaction $M_3(C,B)+\gamma\text{-Fe}\rightarrow M_{23}(C,B)_6+\alpha\text{-Fe}$. The shape of the miscibility gap is elongated in the direction of higher boron contents. Due to this behavior, the stability of the $M_{23}(C,B)_6$ phase strongly depends on the B/(B+C) ratio. In the case of the Fe1C0.2B alloy (***Figure 9a***), the presence of the $M_{23}(C,B)_6$ phase is calculated to be in the temperature range of 900-980°C. In contrast, the temperature range in which the $M_{23}(C,B)_6$ phase is stable is enlarged in the temperature range from 750 to 950°C in the case of adding an additional 0.2 mass% boron (alloy Fe1C0.4B). However, these calculations are in good agreement with the results published in the literature [21,23] for the stability field of the $M_{23}(C,B)_6$ phase. In addition, the shape of the miscibility gap and the huge influence of small variations of added boron might explain the significant differences in the stability range, which are found in the literature [24,25].

The influence of carbon on the stability of the τ phase is shown in ***Figure 9b***, in which the carbon content was increased to 2 mass% in contrast to ***Figure 9a***. The calculations indicate that carbon shifts the miscibility gap (area of the τ phase) in the direction of higher boron contents and to lower temperatures. This behavior can be explained by the stabilizing effect of carbon addition on boron cementite.

The influence of the element Cr on τ phase formation is shown in ***Figure 9c*** and ***9d***. A comparison of the phase diagrams of the alloys Fe-1C-xB (***Figure 9a***) and Fe-1C-0.25Cr-xB

(***Figure 9c***) shows that the phase field of [$M_{23}(C,B)_6$+γ-Fe] is expanded in terms of temperature and boron concentration as a result of adding Cr. Even in the absence of the element boron, formation of $M_{23}C_6$ phase can be observed in a temperature range from 920 to 1120°C. The influence of an increase in the content of carbon as well as chromium is shown in ***Figure 9d***. At a lower boron content, the $M_3(C,B)$ phase is stabilized due to the higher solubility of boron and carbon and lower metal/metalloid ratio between the $M_3(C,B)$ phase (M/X=3) compared to the $M_{23}(C,B)_6$ phase (M/X=3.833). Above a boron content of 0.4 to 0.8 mass%, the $M_{23}(C,B)_6$ phase becomes stable along with $M_3(C,B)$. Furthermore, the stability of the $M_{23}(C,B)_6$ phase is increased in the direction of higher temperatures, thus the $M_{23}(C,B)_6$ phase solidifies eutectically in the Fe-0.1Cr-2C-0.8B alloy. The calculations shown in ***Figure 9*** reveal that decomposition of the $M_{23}(C,B)_6$ phase at lower temperatures is associated with the γ-α transition. The drop in C solubility in the iron phases stabilizes C-richer types of hard phases i.e. the $Fe_3(C,B)$ phase in the low Cr-FeCB alloy,(***Figure 9)***, and the M_7C_3 phase in the high Cr-FeCB alloy. This is discussed later.

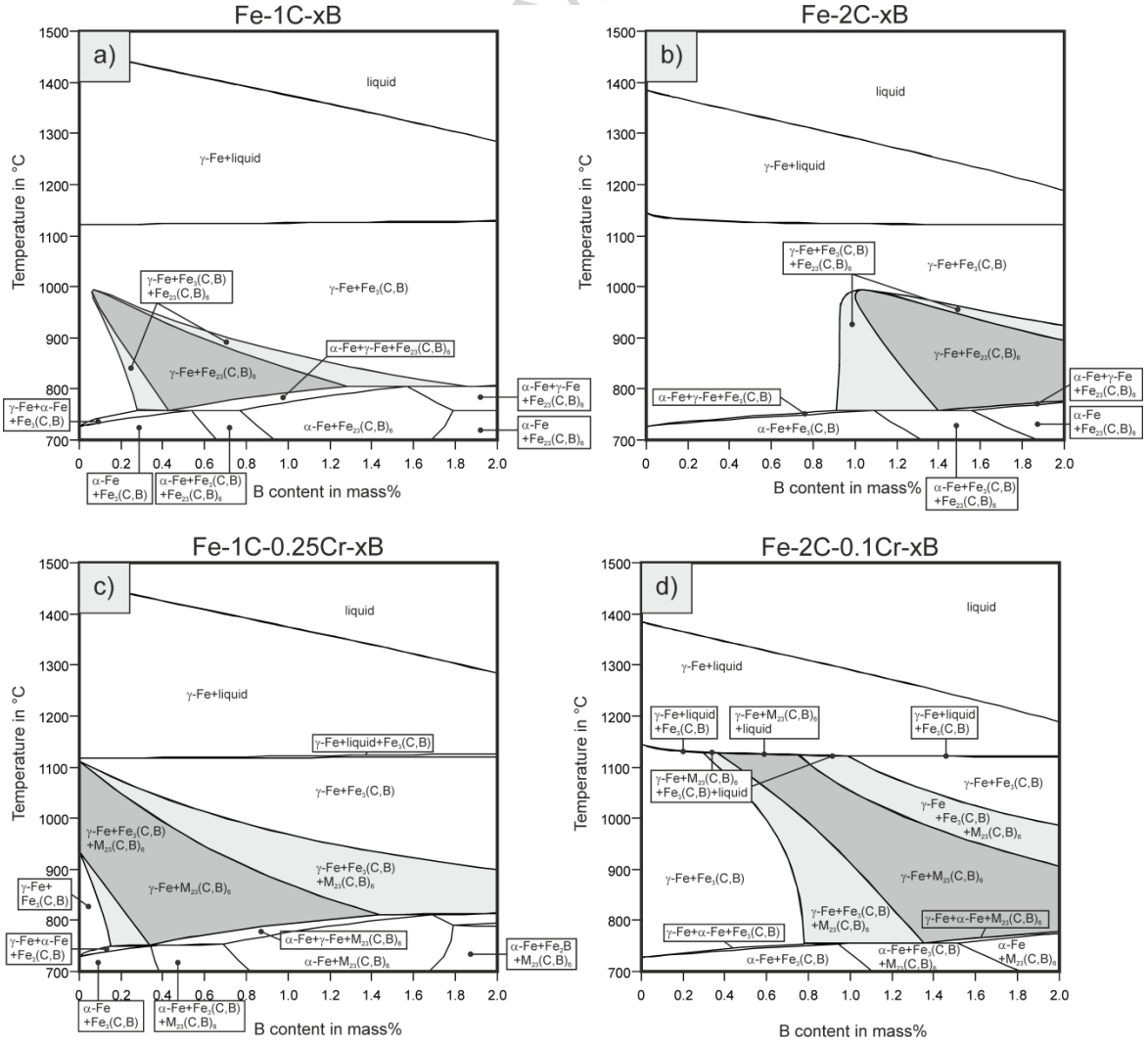

Figure 9: Influence of B/(B+C) ratio and Cr content on the formation of the τ phase ($M_{23}(C,B)_6$) in the Fe-C-B and Fe-C-B-Cr systems

4.3 Formation and transformation of the M_2B

Above an overall Cr content of 7.2 mass%, the primary solidification of γ-Fe in hypoeutectic FeCB-Cr alloys is followed by the formation of both orthorhombic $(Cr,Fe)_2B$ and tetragonal $(Fe,Cr)_2B$ phases and also eutectic crystallization of the $M_{23}(C,B)_6$ phase (***Figure 1***). The orthorhombic $(Cr,Fe)_2B$ phase solidifies before the tetragonal $(Fe,Cr)_2B$, which is attributed to its higher thermodynamic stability. The work of Zhou et al. should be mentioned in this context. They calculated the enthalpy of formation of orthorhombic Cr_2B (ΔH_r=-37.67 kJ/g·atom) and tetragonal Fe_2B (ΔH_r=-24.2 kJ/g·atom.) [26]. In the solid state, the microstructure of the FeCB8Cr and FeCB10Cr specimens consists of a metallic matrix and $(Fe,Cr)_2B$- and $(Cr,Fe)_2B$-type hard phases as well as coral-like, eutectic $M_{23}(C,B)_6$ phases. This is in accordance with equilibrium calculations (***Figure 1, Figure 2***) as well as with experimental phase analysis (***Figure 5)*** and SEM investigations (see FeCB8Cr, and FeCB10Cr specimens in ***Figure 4***).

However, the volume fraction of the hard phases in the solid state is temperature-dependent, as shown for the FeCB8C alloy in ***Figure 10a***. ***Figure 10b*** shows the volume fraction of the $(Cr,Fe)_2B$, $(Fe,Cr)_2B$, and $M_{23}(C,B)_6$ phases as a function of the temperature. A strong decrease in the volume fraction of the $(Fe,Cr)_2B$ phase in the direction of lower temperatures as well as a decrease in solute Cr content in the γ-Fe phase (***Figure 11a***) is observed. Simultaneously, the volume fraction of the $(Cr,Fe)_2B$ and $M_{23}(C,B)_6$ phases increases, which is attributed to solid-state transformations relating to the schematic reaction $(Fe,Cr)_2B+\gamma\text{-}Fe \rightarrow (Cr,Fe)_2B+M_{23}(C,B)_6$. Thus the $(Fe,Cr)_2B \rightarrow (Cr,Fe)_2B$ transformation has to be discussed based on the solubility of the element Cr and the crystallographic structure of the respective phases [18]. The EDS investigations revealed that the solubility limit of Cr in the $(Fe,Cr)_2B$ phase is close to 17.5 mass%, which is in good agreement with calculations that give a Cr solubility of 16 mass% in tetragonal $(Fe,Cr)_2B$ at 900 °C (***Figure 11b***) and also with the work of *Chrisodoulou and Yijian et al.* who found a maximum solubility of 16-17 mass% Cr inside the Fe-rich tetragonal $(Fe,Cr)_2B$ phase [13,14]. In contrast, the work of Kaneko *et al.* found that the solubility of Fe in the orthorhombic $(Cr,Fe)_2B$ phase is much higher than the solubility of Cr in the tetragonal $(Fe,Cr)_2B$ phase [23]. Taking account of the solubility limit of Cr and Fe as well as the similarity of the crystallographic structures of $(Cr,Fe)_2B$ and $(Fe,Cr)_2B$, a transformation of tetragonal $(Fe,Cr)_2B$ to orthorhombic $(Cr,Fe)_2B$ will occur if the Cr content inside the M_2B phase exceeds the Cr solubility due to short-range diffusion of the elements Cr and Fe. Thus, a decrease in the solute Cr content of the γ-Fe phase (***Figure 11a)*** is

coupled to the reaction $(Fe,Cr)_2B+\gamma\text{-}Fe \rightarrow (Cr,Fe)_2B+M_{23}(C,B)_6$ ***(Figure 10).*** Furthermore, the calculations show that the solute Cr content inside the $(Cr,Fe)_2B$ phase increases from 26 mass% at 900 °C to 33 mass% at 600 °C as the temperature decreases (***Figure 11b***), whereas the Cr content inside the iron phases (γ-Fe and α-Fe) simultaneously decreases (***Figure 11a***). The microstructural transformation process of $(Fe,Cr)_2B \rightarrow (Cr,Fe)_2B$ was investigated in detail by *Lin et al.* and *Goldfarb et al.* by means of TEM investigations [12,13]. They assumed that the $(Fe,Cr)_2B \rightarrow (Cr,Fe)_2B$ transformation mechanism is atom substitution and structural adjustments, which should be possible due to the similarity between the structure of the tetragonal and orthorhombic M_2B-type phases. They found tetragonal $(Fe,Cr)_2B$ phases as a kind of stacking fault in the form of thinly sliced sandwiches between (100) faces of orthorhombic $(Cr,Fe)_2B$ phases, thus allowing the coexistence of $(Fe,Cr)_2B$ and $(Cr,Fe)_2B$ due to its polytypism behavior. This means that the $(Fe,Cr)_2B \rightarrow (Cr,Fe)_2B$ transformation can be attributed to a similarity of the crystallographic structure between both M_2B phases. Thus, if the solubility of Cr in the tetragonal $(Fe,Cr)_2B$ phase is exceeded, orthorhombic $(Cr,Fe)_2B$ is formed by atomic shifts of boron on the {110} crystallographic planes. Thus heterogeneous nucleation of $(Cr,Fe)_2B$ occurs at the previously formed stacking faults in $(Fe,Cr)_2B$ [12].

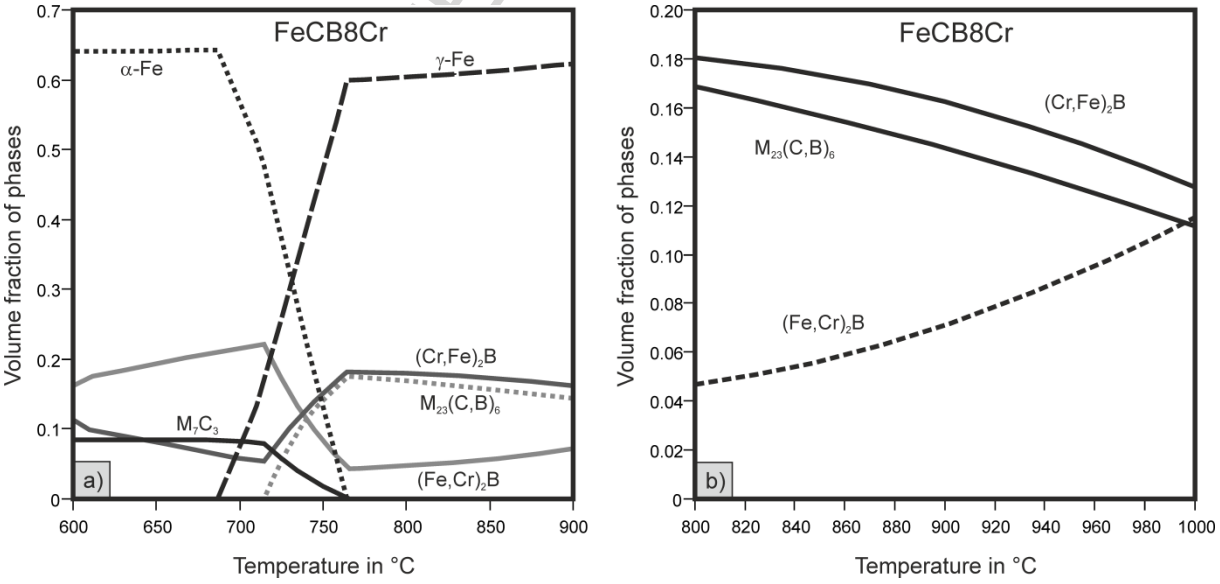

Figure 10: a) M_7C_3 formation in the equilibrium state by transformation of the hard phases $(Cr,Fe)_2B$ and $M_{23}(C,B)_6$ at the γ-α transition; b) volume fraction of M_2B and $M_{23}(C,B)_6$-type hard phases in the FeCB8Cr alloy as a function of temperature

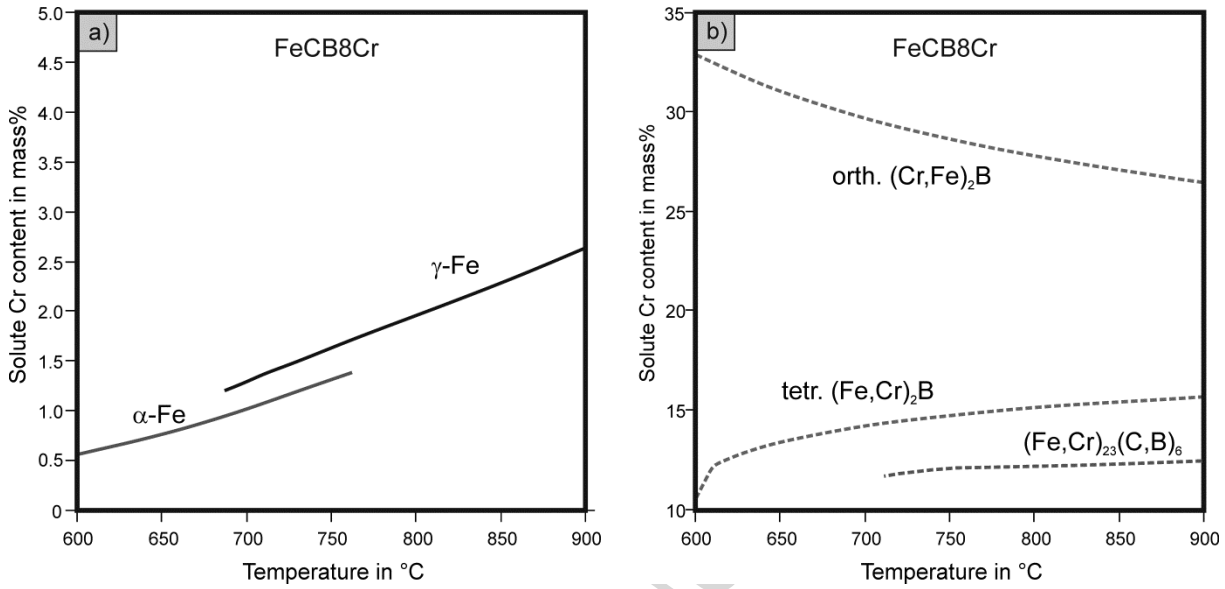

Figure 11: Solute Cr content a) in α-Fe and γ-Fe phases; b) in $(Cr,Fe)_2B$ and $(Fe,Cr)_2B$ phases for the FeCB8Cr alloy as a function of temperature

When the overall Cr content was higher than 9.2 mass%, only orthorhombic $(Cr,Fe)_2B$ and no tetragonal $(Fe,Cr)_2B$ phases were found in the liquid as well as in the solid state above temperatures of 800°C by the calculations shown in ***Figure 1***. The associated solidification sequence is characterized by primary solidification of γ-Fe metal cells followed by the formation of orthorhombic $(Cr,Fe)_2B$-type hard phases and eutectic crystallization of the $M_{23}(C,B)_6$ phase. This behavior is attributed to the high Cr content. Thus, the Cr content in the M_2B phases exceeds the solubility limit in tetragonal $(Fe,Cr)_2B$ and thus counteracts its formation and stabilizes the orthorhombic $(Cr,Fe)_2B$ type.

4.4 Formation and transformation of the M_7C_3 phases

It can be gathered from the literature that, in the case of Fe-C-B-Cr alloys, formation of Cr-rich M_7C_3 carbide can be observed [27]. In our work, M_7C_3 was not observed in the microstructure of the laboratory melts nor in the thermodynamic calculations performed in the temperature range from 800 to 1400°C, which represents the austenitic stability range. This behavior can be explained by the binding of Cr in the M_2B and $M_{23}(C,B)_6$ phases and of C in the $M_{23}(C,B)_6$ and γ-Fe phases. However, in the direction of lower temperatures, the solubility of C in the metal matrix decreases and the $M_{23}(C,B)_6$ phases dissolve, which thus promotes the formation of Cr-rich M_7C_3 carbides. In ***Figure 10a***, the formation of Cr-rich M_7C_3 carbides with respect to the FeCB8Cr alloy at lower temperatures is illustrated by means of thermodynamic calculations. The calculations indicate a solute Cr content inside the Cr-rich M_7C_3 phase that is slightly decreasing with temperature from 40 mass% at 760 °C to 37

mass % at 600°C. Thus the M_7C_3 phase formation is attributed to the γ-α transus, dissolution of the $M_{23}(C,B)_6$ phase, and a "re-transformation" of orthorhombic $(Cr,Fe)_2B$ to tetragonal $(Fe,Cr)_2B$. The release of the elements Cr and especially C from γ-Fe due to the γ-α transformation is thermodynamically stabilizing the C- and Cr-rich M_7C_3-type carbide with a lower metal/metalloid ratio of M/C = 2.33 as compared to $M_{23}C_6$ (M/C = 3.833). Therefore, formation of the M_7C_3-type carbide requires redistribution of the element Cr and is accompanied by the dissolution of the $M_{23}(C,B)_6$ phase, which is less favorable in terms of metal/metalloid ratio. In turn, dissolution of the $M_{23}(C,B)_6$ phase provides the elements Cr, Fe, and also C. Hence, both the dissolution of $M_{23}(C,B)_6$ and the formation of the M_7C_3 phase start simultaneously on reaching the γ-α transus temperature. In addition, thermodynamic calculations reveal a decrease in the volume fraction of the orthorhombic $(Cr,Fe)_2B$ phase with a simultaneous increase in the M_7C_3 phase (***Figure 10a***). In this manner, the dissolution of the $(Cr,Fe)_2B$ phase also acts as Cr donor and supports the formation of the Cr-rich M_7C_3 phase. Nevertheless, the solute Cr content inside the $(Cr,Fe)_2B$ increases with decreasing temperatures in spite of the formation of the Cr-rich M_7C_3 phase (***Figure 11b)***. However, the solubility of boron in the M_7C_3 phase and in the bcc metal matrix can be neglected. Thus, large portions of the orthorhombic $(Cr,Fe)_2B$ phase transform to the tetragonal $(Fe,Cr)_2B$ phase due to substitution of Cr lattice sites by Fe atoms. Furthermore, as a consequence of the release of B due to dissolution of the $M_{23}(C,B)_6$ phase, the volume fraction of M_2B-type phases (sum of $(Cr,Fe)_2B$ + $(Fe,Cr)_2B$ phases) increases from 23 vol% up to 27 vol% at temperatures below the γ-α transition. Apart from that, the volume fraction of M_2B-type phases is temperature-independent and remains at a constant level, whereas the fraction of the particular $(Cr,Fe)_2B$ or $(Fe,Cr)_2B$ phases is changing due to the $(Fe,Cr)_2B \leftrightarrow (Cr,Fe)_2B$ transformation. Finally, it can be pointed out that M_7C_3 formation occurs concurrently with the γ-α transus and is not only attributed to dissolution of the $M_{23}(C,B)_6$ phase and the Cr release of the iron matrix phases, but also requires the transformation of the $(Cr,Fe)_2B \rightarrow (Fe,Cr)_2B$ phase.

4.5 Influence of Cr addition on hard phase properties

For an equal metal M to metalloid X stoichiometry, borides usually possess a higher hardness than carbides or nitrides (X = B, C or N). This is attributed to stronger M-B and B-B bonding behavior. The hardness of Zr-rich mono hard phases should be mentioned as an example: The hardness decreases from the boride (ZrB ~3600 HV0.05) to the carbide (ZrC ~2600 HV0.05) and then to the nitride (ZrN ~1300-2000 HV0.05) [28].

In addition to a higher hardness, borides possess excellent mechanical and chemical properties (Young's modulus, toughness, corrosion resistance), which illustrate the motivation for the use of borides as hard phases in wear-resistant materials such as hardfacing alloys, tool steels, or white cast irons. The work of Xiao et al. compared the material properties of Fe_2B, Cr_7C_3, and Fe_3C by means of DFT calculations and indentation experiments [29]. They found highest hardness for pure Cr_7C_3. In contrast, the measured hardness of pure Fe_2B was in the range of 1400 HV, which is close to the hardness of pure Cr_7C_3. Nevertheless, they also found an increase in hardness and Young's modulus by doping the Fe_2B phase with transition metals from the fourth to sixth subgroups. Oezdemir et al. reported for Fe_2B a hardness close to a value of 1700 HV and a low fracture toughness of 3.59 to 3.83 MPa√m [30]. Huang et al. reported an increase in hardness as well as fracture toughness for the tetragonal $(Fe,Cr)_2B$ phase in the direction of a higher solute Cr content: The hardness increased from 1560 HV1 (0 mass% Cr in M_2B) to 1670 HV1 (~6 mass% Cr in M_2B) and the fracture toughness increased from 3.8 to ~7-8 MPa√m [31]. Our work confirms the increase in hardness on doping Fe_2B as well as $Fe_{23}(C,B)_6$ with Cr, as shown in ***Figure 6***. In this case, the hardness increases on increasing the overall Cr content in the alloy, although the influence of Cr addition on the increase in hardness of the $M_{23}(C,B)_6$ phase is less pronounced and will therefore not be discussed intensively.

The increase in hardness due to doping the tetragonal M_2B phase with transition elements is attributed to a change in the bonding behavior, which is associated with a change in the electron configuration [32]. The bonding behavior of monoborides (MB) and hemiborides (M_2B) is usually discussed in the context of the presence of M-B, B-B, and M-M bonds, whereby the respective bonding strength is determined by transfer of delocalized valence electrons of the transition metal to the boron atoms. The formation of Fe-rich monoborides or hemiborides has been attributed to the formation of sp^2 configurations of the boron atoms. In the case of higher borides, sp3 configurations are present [33]. This sp2/sp3 configuration and thus the bonding are affected by the participating behavior of the delocalized valence electrons of the transition element. In the case of Fe (3d24s2), formation of the stable d5 configuration can act as a donor electron. Thus, sp2-hybridization of the boron atoms leads to strong covalent B-Fe bonding between the sp2 (B) and d5 (Fe) configurations, which results in a high hardness of the Fe2B boride phase. However, the improvement in hardness of the M2B phase due to an increase in Cr content has to be discussed differently. In the case of small Cr additions in which the tetragonal (Fe,Cr)2B phase is present, Fe is replaced by Cr atoms in the M2B lattice. Fe substitution by Cr ($3d^54s^1$) is accompanied by an increase in the B-B bond energy between the boron atoms in the [002] direction by increasing the amount of shared electron pairs [31]. This increase in bond energy between B-B is then accompanied by an increase in hardness. In the direction of a higher solute Cr content in

M_2B of 12-17.5 mass%, the hardness was further increased. We assume that this increase in hardness can be attributed to the coexistence of the tetragonal $(Fe,Cr)_2B$ phase and the orthorhombic $(Cr,Fe)_2B$ phase, which has been reported by Ma et al. for Fe-3.5B-5Cr and Fe-3.5B-8Cr alloy [16]. Exceeding the solubility limit of Cr in the tetragonal $(Fe,Cr)_2B$ phase leads to the formation of the orthorhombic $(Cr,Fe)_2B$ phase. This means that the tetragonal $(Fe,Cr)_2B$ and orthorhombic $(Cr,Fe)_2B$ phases coexist in this range, which was confirmed by XRD investigations (***Figure 5***) and the measured values of the Young´s modulus of the M_2B phase with increasing Cr content (***Figure 7***). The increase in hardness can thus be attributed to the effects of an increased Cr content in tetragonal $(Fe,Cr)_2B$ phase as well as to formation of the orthorhombic $(Cr,Fe)_2B$ phase, which exhibits a higher hardness than tetragonal $(Fe,Cr)_2B$. The hardness of orthorhombic Cr-rich $(Cr,Fe)_2B$ was investigated by Ma et al. They measured a hardness of >1690 HV0.1, which exceeds the hardness of Cr-rich M_7C_3, which is a well-known hard phase in cast irons or tool steels. The higher hardness of Cr_2B can be explained by the work of Zhou et al., who investigated the bonding behavior of the transition elements Cr, Co, Fe, Ni, Mo, and W in X_2B by means of ab initio calculations [26]. Especially for the compound Cr_2B, they found an increased M-B and M-M bonding compared to Fe_2B. Compounds with a high bonding energy commonly have a high melting point and enhanced mechanical properties such as strength, Young´s modulus, and hardness.

In the case of the analyzed alloys with an overall Cr content of up to 4 mass%, no change in the Young's modulus of the $(Fe,Cr)_2B$ phase was recognized ***(Figure 7)***. If the overall Cr content is increased above 4 mass%, a steady rise in the Young's modulus of M_2B-type phases can be observed, reaching a maximum Young's modulus of 390 GPa at 10 mass% overall Cr content. We utilized the increase in the Young's modulus as an indicator of the increase in bonding strength in M_2B-type phases and thus for the fraction of $(Fe,Cr)_2B \rightarrow (Cr,Fe)_2B$ transformation. This implies that the formation of $(Cr,Fe)_2B$ starts at an overall Cr content between 4 and 6 mass%. We thus interpret the steady rise in Young's modulus by a constant increase in the volume fraction of Cr_2B due to the $(Fe,Cr)_2B \leftrightarrow (Cr,Fe)_2B$ transformation, for which the overall volume fraction of M_2B phases remains at a constant level in the range of 4 to 10 mass% Cr. The same applies to the Cr content inside the $(Cr,Fe)_2B$ phase, which is lower as measured using EDS (***Figure 6*** and ***Figure 7***) compared to the calculated values for alloys having a Cr content > 6 mass% (***Figure 11b***). Furthermore, the coexistence of the orthorhombic Cr_2B and tetragonal Fe_2B phases is confirmed by the XRD measurement of the FeCB6Cr alloy (***Figure 5***). However, this is in disagreement with the calculations (***Figure 2***), which indicate that the Cr_2B phase is not thermodynamically stable below a Cr content of 6.8 mass%. The discrepancies between the calculated and experimentally observed microstructures might be due to in-equilibrium

effects on solidification and solid-state transformations as well as the inaccuracy of the used database.

In the case of the $(Fe,Cr)_{23}C_6$ phase, it can be seen that an increase in the solute Cr content has a minor effect on the hardness evolution. The same behavior applies in the case of the Young's modulus.

4.6 Alloy design

It is evident from the presented results that Cr-rich $(Cr,Fe)_2B$ borides possess excellent mechanical properties such as hardness (up to 2000 HV), Young's modulus (up to 390 GPa) (see ***Figure 6*** and ***Figure 7***), as well as an increased fracture toughness (up to ≥ 20 MPa√m [16]). Therefore, utilization of Cr-rich $(Cr,Fe)_2B$ hard phases for wear-resistant Fe-base alloys is of high technological interest, and the aim of future alloy developments will be to stabilize the orthorhombic $(Cr,Fe)_2B$ phase. In this context, the experimental results indicate that the $(Cr,Fe)_2B$ phase is present in the microstructure at Cr contents > 4 mass%, which is lower than the value determined by calculation (>6.8 mass%). This is favorable in terms of cost, because the amount of Cr required to stabilize the $(Cr,Fe)_2B$ phase is lower than the calculated value. However, it was also shown that Cr stabilizes the τ phase $[(Fe,Cr)_{23}(C,B)_6]$, which possesses a low hardness (1100 to 1250 HV) and a low Young's modulus (280 to 300 GPa), which thus counteract the high resistance to abrasive wear. In addition, the τ phase chemically binds the alloying element Cr and, consequently, reduces the effective Cr content required for the formation of $(Cr,Fe)_2B$ borides. Simultaneously, the τ phase also binds the element C. This affects the C content inside the γ-Fe matrix, which is required for martensitic hardening and thus the hardening temperature chosen for this study was a comparatively high value of 900 °C. Accordingly, further work will focus on destabilization of the τ phase in consideration of the alloying design. This would allow a lower hardening temperature, which would lead to energy savings as well as a higher Cr content inside the $(Cr,Fe)_2B$ phase and thus improved mechanical properties (see ***Figure* 11b** and ***Figure* 7)**. Thus elements such as vanadium, molybdenum, and tungsten as well as the manganese and silicon considered in this study are of great interest due to their stabilizing impact on the M_2B phase and their destabilizing effect on the τ phase. Furthermore, the elements Mo and W, in particular, are promising for increasing the hardness of the M_2B-type phases because their electron configuration is larger and they thus provide more electrons that can participate in covalent bonding [32,33].

5. Summary and Conclusion

The present paper focuses on the influence of the element Cr on the microstructural evolution of hypoeutectic FeCB-Cr alloys and on the corresponding phase properties with the objective to give advice for the development of steels within this alloying system. Therefore, the Fe0.75C2B-Cr system having 2.5 mass% Si and 3.8 mass% Mn was mapped by thermodynamic calculations, which were then verified by comparing them with experimental data. Laboratory melts were produced, and the microstructure was analyzed with respect to the influence of Cr on the phase composition (XRD) and solute Cr content in the respective phases (EDS). Particular attention was paid to the influence of Cr content on hard phase formation and the associated mechanical properties of the hard phase such as hardness and Young's modulus (nanoindentation experiments).

- The hypoeutectic composition of the analyzed Fe0.75C2B-Cr alloys shows primary solidification of γ-Fe. Depending on the Cr content, solidification of γ-Fe is followed by the formation of different phases from the melt: $(Fe,Cr)_2B$ (Cr < 7.2 mass%); $(Cr,Fe)_2B$+$(Fe,Cr)_2B$ (7.2 mass% < Cr < 8.8 mass%), or $(Cr,Fe)_2B$ (8.8 mass% < Cr). The low-melting eutectic phase is $Fe_3(C,B)$ (Cr < 3 mass%) or $M_{23}(C,B)_6$ (Cr > 3 mass%).
- A stabilizing effect of Cr addition was found for $M_{23}(C,B)_6$ formation. The $M_{23}(C,B)_6$ phase is also formed due to solid-state transformation above Cr contents > 1.8 mass% at a hardening temperature of 900 °C. The element C was found to shift the phase field of $M_{23}(C,B)_6$ stability to higher B contents.
- Formation of the orthorhombic $(Cr,Fe)_2B$ phase is promoted by Cr addition. A Cr content of 4-6 mass% was observed to stabilize the $(Cr,Fe)_2B$ phase in experiments, in contrast to the calculated value of > 6.8 mass% Cr required to form $(Cr,Fe)_2B$.
- Transformation of $(Fe,Cr)_2B \rightarrow (Cr,Fe)_2B$ occurs in the stability region of γ-Fe (hardening temperature) at decreasing temperatures, whereas the volume fraction of the $(Fe,Cr)_{23}(C,B)_6$ phase increases. The $(Cr,Fe)_2B$ and $(Fe,Cr)_2B$ phases coexist, whereas the fraction of both M_2B-type phases remains at a constant level of 23 vol.%.
- The Cr content inside the $(Cr,Fe)_2B$ increases with decreasing temperature, whereas the Cr content inside the γ-Fe and α-Fe phases simultaneously decreases.
- The formation of α-Fe at temperatures falling below the γ-α transition stabilizes the Cr- and C-rich M_7C_3 phase in the case of high-Cr FeCB alloys. The $(Fe,Cr)_{23}(C,B)_6$ phase is less favorable in terms of the metal/metalloid ratio (M/X: $M_{23}(C,B)_6$ = 3.833 > M_7C_3 = 2.333) and thus is dissolving. This acts as a Cr and C donor for the formation of the M_7C_3 phase. Moreover, the fraction of the $(Cr,Fe)_2B$ phase decreases and a retransformation of $(Cr,Fe)_2B \rightarrow (Fe,Cr)_2B$ occurs, which makes the element Cr available. Furthermore, as a consequence of the release of B associated with the dissolution of the $M_{23}(C,B)_6$ phase, the volume fraction of the M_2B-type phases (sum

of $(Cr,Fe)_2B$ + $(Fe,Cr)_2B$ phases) increases from 23 vol.% up to 27 vol.% at temperatures below the γ-α transition.

- Cr addition was found to induce an increase in hardness (up to 2000 HV) and Young's modulus (up to 390 GPa) simultaneously with the $(Fe,Cr)_2B \rightarrow (Cr,Fe)_2B$ phase transition. The improvement in the mechanical properties is attributed to substitution of Fe atoms by Cr atoms inside the $(Cr,Fe)_2B$ crystal structure, which is associated with a strengthening of the covalent bonding behavior.
- Due to the high hardness and Young's modulus, the $(Cr,Fe)_2B$ boride is of high technological interest for future alloy development. However, the simultaneous Cr addition to the $(Cr,Fe)_2B$ phase stabilizes the $M_{23}(C,B)_6$ phase, which leads to poor mechanical properties and also binds the elements Cr and C. Therefore, further alloy development should focus on preventing formation of the $M_{23}(C,B)_6$ phase by alloying with Mn, Si, V, W, and Mo.

6. Acknowledgements

The authors gratefully acknowledge financial support from the "Deutsche Forschungsgemeinschaft" (DFG) within the project "boron-alloyed tool steels" RO 4523/2-1.

7. References

[1] Sasaki T, Yakou T, Umemoto M, Todaka Y. Wear 2006;260:1090–5.
[2] Shafirstien G, Bamberger M, Langohr M, Maisenhalder F. Surface and Coatings Technology 1991;45:417–23.
[3] Kagawa A, Okamoto T. J. Mater. Sci. 1983;18:225–30.
[4] Lentz J, Röttger A, Theisen W. Gefügeausbildung und mikromechanische Eigenschaften einzelner Phasen von untereutektischen Fe-C-B Legierungen, in: Mayer S, Panzenböck M, Clemens H (Eds.). Fortschritte in der Metallographie. Bonn: INVENTUM GmbH; 2014. p. 283–288.
[5] Shein IR, Medvedeva NI, Ivanovskii AL. Physica B: Condensed Matter 2006;371:126–32.
[6] Sahin S, Meric C. Materials Research Bulletin 2002;37:971–9.
[7] Röttger A, Weber S, Theisen W. Mat. Sci. and Eng.: A 2012;532:511–21.
[8] Gunduz KO, Gencer Y, Tarakci M, Calik A. Surface and Coatings Technology 2013;221:104–10.
[9] Campos-Silva I, Ortiz-Domínguez M, Bravo-Bárcenas O, Doñu-Ruiz MA, Bravo-Bárcenas D, Tapia-Quintero C, Jiménez-Reyes MY. Surface and Coatings Technology 2010;205:403–12.
[10] Berns H, Saltykova A, Röttger A, Heger D. Steel Res Int. 2011;82:786–94.

[11] Rogl P. Boron – Carbon – Iron, in: Martienssen W, Effenberg G, Ilyenko S (Eds.). Iron Systems, Part 1. Berlin, Heidelberg: Springer Berlin Heidelberg; 2008. p. 349–378.

[12] Goldfarb I, Kaplan WD, Ariely S, Bamberger M. Philosophical Magazine A 1995;72:963–79.

[13] Yijian L, Jian H. J Mater Sci 1991;26:2833–40.

[14] Christodoulou P, Calos N. Materials Science and Engineering: A 2001;301:103–17.

[15] Dybkov VI, Goncharuk LV, Khoruzha VG, Meleshevich KA, Samelyuk AV, Sidorko VR. Solid State Phenomena 2008;138:181–8.

[16] Ma S, Xing J, Liu G, Yi D, Fu H, Zhang J, Li Y. Materials Science and Engineering: A 2010;527:6800–8.

[17] Feng J, Xiao B, Zhou R, Jiang YH, Cen QH. Procedia Engineering 2012;31:676–81.

[18] Medvedeva NI, van Aken DC, Medvedeva JE. Computational Materials Science 2015;96:159–64.

[19] Lentz J, Röttger A, Theisen W. Acta Materialia 2015;99:119–29.

[20] Li L, Wang W, Hu L, Wei B. Intermetallics 2014;46:211–21.

[21] Schürmann E, Shao-Xiong L. Giessereiforschung 1985;37:121–9.

[22] Poletti MG, Battezzati L. Calphad 2013;43:40–7.

[23] Kaneko H, Nishizawa T, Chiba A. J. Japan Inst. Metals 1966;30:263–9.

[24] Borlera ML, Pradelli G. Metall. Ital. 1987;59:907.

[25] Stadelmaier H, Gregg R. Metall. 1963;17:412–4.

[26] Zhou CT, Xing JD, Xiao B, Feng J, Xie XJ, Chen YH. Computational Materials Science 2009;44:1056–64.

[27] Hartono W, Aso S, Goto S., Kamatsu Y. Int. J. Soc. Mater. Eng. Resour. 2002;10:99–105.

[28] C. Friedrich, G. Berg, E. Broszeit, C. Berger, Friedrich C, Berg G, Broszeit E, Berger C. Mat.-wiss. u. Werkstofftech 1997;28:59–76.

[29] Xiao B, Xing JD, Feng J, Li YF, Zhou CT, Su W, Xie XJ et al. Physica B: Condensed Matter 2008;403:2273–81.

[30] Ozdemir O, Usta M, Bindal C, Ucisik A. Vacuum 2006;80:1391–5.

[31] Huang Z, Xing J, Guo C. Materials & Design 2010;31:3084–9.

[32] Suwattananont N, Petrova R. Solid State Sciences 2012;14:1669–72.

[33] Shveikin GP, Ivanovskii AL. Russian Chemical Reviews 1994;63:711–34.

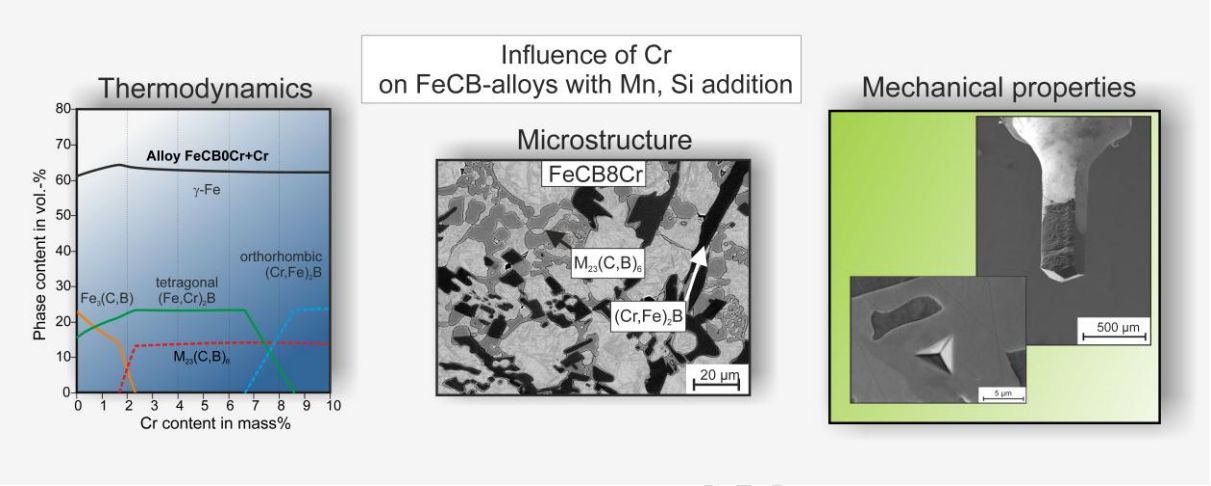

Graphical abstract

Highlights

- Influence of Cr-addition on Fe0.75C2B alloy with Mn and Si addition is analyzed
- Cr promotes the formation of M_2B
- $(Fe,Cr)_2B \rightarrow (Cr,Fe)_2B$ phase transition occures at higher Cr addition
- Mechanical properties of M_2B phase are improved with increasing Cr content
- $(Cr,Fe)_2B$ phase is of high technological interest for future alloy development